frontiers | Frontiers in Bioengineering and Biotechnology

TYPE Review
PUBLISHED 24 August 2022
DOI 10.3389/fbioe.2022.984336

OPEN ACCESS

EDITED BY
Piera Di Martino,
University of Camerino, Italy

REVIEWED BY
Siavash Iravani,
Isfahan University of Medical Sciences, Iran
Xianwen Wang,
Anhui Medical University, China

*CORRESPONDENCE
Majid Rezayi,
rezaeimj@mums.ac.ir
Majid Khazaei,
khazaeim@mums.ac.ir

SPECIALTY SECTION
This article was submitted to Nanobiotechnology, a section of the journal Frontiers in Bioengineering and Biotechnology

RECEIVED 01 July 2022
ACCEPTED 26 July 2022
PUBLISHED 24 August 2022

CITATION
Ranjbari S, Darroudi M, Hatamluyi B, Arefinia R, Aghaee-Bakhtiari SH, Rezayi M and Khazaei M (2022), Application of MXene in the diagnosis and treatment of breast cancer: A critical overview.
Front. Bioeng. Biotechnol. 10:984336.
doi: 10.3389/fbioe.2022.984336

Application of MXene in the diagnosis and treatment of breast cancer: A critical overview

Sara Ranjbari[1], Mahdieh Darroudi[2,3], Behnaz Hatamluyi[4], Reza Arefinia[1], Seyed Hamid Aghaee-Bakhtiari[3], Majid Rezayi[3,5,6]* and Majid Khazaei[2,6]*

[1]Chemical Engineering Department, Faculty of Engineering, Ferdowsi University of Mashhad, Mashhad, Iran, [2]Department of Physiology, Faculty of Medicine, Mashhad University of Medical Science, Mashhad, Iran, [3]Department of Medical Biotechnology and Nanotechnology, School of Science, Mashhad University of Medical Science, Mashhad, Iran, [4]Department of Pharmacology, Faculty of Medicine, Mashhad University of Medical Sciences, Mashhad, Iran, [5]Medical Toxicology Research Center, Mashhad University of Medical Science, Mashhad, Iran, [6]Metabolic Syndrome Research Center, Mashhad University of Medical Science, Mashhad, Iran

Breast cancer is the second most common cancer worldwide. Prognosis and timely treatment can reduce the illness or improve it. The use of nanomaterials leads to timely diagnosis and effective treatment. MXenes are a 2D material with a unique composition of attributes, containing significant electrical conductance, high optical characteristics, mechanical consistency, and excellent optical properties. Current advances and insights show that MXene is far more promising in biotechnology applications than current nanobiotechnology systems. MXenes have various applications in biotechnology and biomedicine, such as drug delivery/loading, biosensor, cancer treatment, and bioimaging programs due to their high surface area, excellent biocompatibility, and physicochemical properties. Surface modifications MXenes are not only biocompatible but also have multifunctional properties, such as aiming ligands for preferential agglomeration at the tumor sites for photothermal treatment. Studies have shown that these nanostructures, detection, and breast cancer therapy are more acceptable than present nanosystems in *in vivo* and *in vitro*. This review article aims to investigate the structure of MXene, its various synthesis methods, its application to cancer diagnosis, cytotoxicity, biodegradability, and cancer treatment by the photothermal process (*in-vivo* and *in-vitro*).

KEYWORDS

biosensor, biomedicine, advanced nanomaterials, biomedical analysis, cancer treatment, breast cancer, MXene

1 Introduction

According to the World Health Organization, breast cancer has the second-highest prevalence of cancer worldwide, with nearly two million breast cancers diagnosed in 2018 (Mittal et al., 2017; Senel et al., 2019; Nazari et al., 2021). Like other cancers, breast cancer occurs when breast cells begin to grow out of control (Waks and Winer, 2019). A

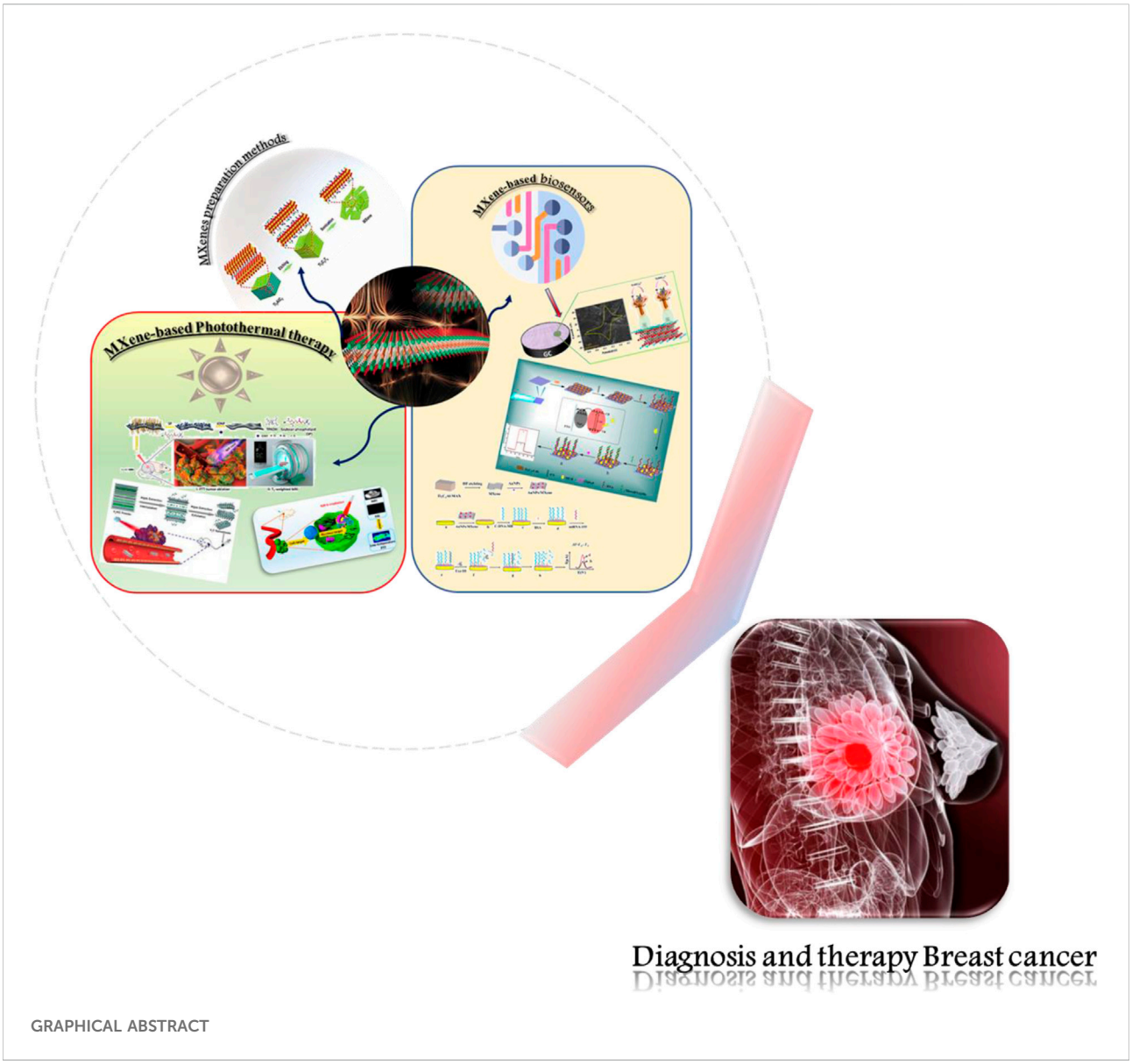

GRAPHICAL ABSTRACT

few changes in the nipple and discoloration of the breast can be symptoms of breast cancer. Also, cancer cells are found mainly in the breast and the lymph nodes in the armpit and armpit (Becker, 2015; Waks and Winer, 2019). Stages 1–4 are dedicated to breast cancer, depending on where the tumor is found. In stage 4, metastatic breast cancer, cells have spread to other places in the body away from the mammary and axillary lymph nodes (Waks and Winer, 2019).

According to different types of proteins in a cell, this type of cancer is classified into three types. 70% of breast cancers involve Hormone-positive receptors that have a progesterone receptor (PR) or estrogen receptor (ER) on the cancer cell (Waks and Winer, 2019). About 15%–20% of breast cancers involve the HER2 + receptor, now known as ERBB2 +, and about 15% of breast cancers are triple-negative and do not have ER, PR, or ERBB2 protein in the cancer cells. The prognosis and therapy of this cancer depend on the type of cancer and its stage (Waks and Winer, 2019). Primarily, breast cancer therapy includes medications, chemotherapy, radiation, and surgery to remove cancer cells from the human body (DeSantis et al., 2019; Tabadkani et al., 2021). Because multiple agents are implicated at the beginning of cancer, these agents can show different signs depending on the kind and place of the tumor. Consequently, the remedy requires early diagnosis, efficient therapy methods, and post-remedy care to prevent relapse (Ali et al., 2015).

Today, nanoparticles such as Au, Ag, CNT, graphene oxide, QDs, MXene, etc., are used in biomedicine and cancer treatment (Wang et al., 2021a; Darroudi et al., 2021; Ma

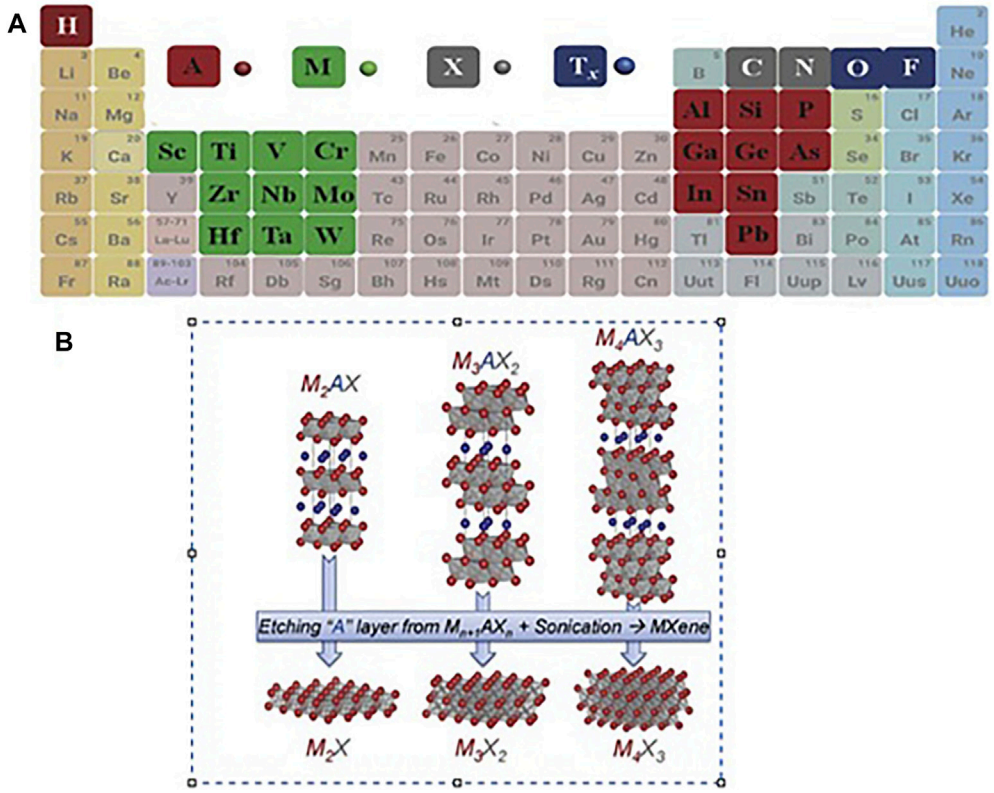

FIGURE 1
(A) Periodic table of the elements utilized from MAX phases (Wang et al., 2018), **(B)** Image of etching layers A from the corresponding MAX phases (Naguib et al., 2014).

et al., 2022). Nanotechnology study, design, and fabrication of nanoscale materials or machines with petite lengths (10^{-9} m) are helpful for various applications. The nanoparticles' properties differ from bulk materials due to their excellent surface area and small dimensions. The chemical, physical, optical, and electronic material properties change with the shape, area, and size of the particles that make them up. These excellent features allow them to show outstanding performance in diagnosing and/or efficient treating various diseases, such as cancer, based on fine-tuning their morphology, surface characteristics, and size (Salata, 2004; Majeed et al., 2019; Qi et al., 2019). MXenes (transfer metal carbides), as 2D (two dimensions) materials, have broad properties such as extensive surface area, high conductivity, and excellent photothermal conversion yield, along with powerful absorption in the NIR area (near-infrared) (Rasool et al., 2016; Pandey et al., 2018; George and Kandasubramanian, 2020). MXenes can be used in a wide range of medical fields like drug delivery (Han et al., 2018; Zhang et al., 2020; Zhu et al., 2021), biomedicine, cancer treatment (Lin et al., 2017; Yu et al., 2017), anti-bacterial (Rasool et al., 2016; Jastrzębska et al., 2019), and diagnosis (Lin et al., 2018; Shurbaji et al., 2021).

This review article aims to examine the structure of MXene, various methods of its synthesis, and its application to cancer diagnosis and cancer treatment by the photothermal process (*in-vivo* and *in-vitro*). In section, the photothermal process addressed the issues of cytotoxicity and biodegradability.

2 MXenes preparation methods

Materials such as graphene with a 2D (Two-dimensional) layer structure have been noted in their particular structure (Tang et al., 2013). High surface area, functional surface, electrical conductivity (Karlsson et al., 2015), and optical properties (Nicolosi et al., 2013). In 2011 Naguib and Gogotsi et al. (2015) at Drexel University discovered 2D Ti_3C_2 powder (Titanium carbide), the MXene household's first candidate (Naguib et al., 2011a; Naguib et al., 2014). MXenes have unique structural and electronic features, making them one of the eldest families of two-dimensional materials used for different applications (Sobolčiak et al., 2019). These materials are of the chemically etched metal carbonitrides and carbides, which have the generic formula

TABLE 1 Various types of MXenes synthesis methods.

Types of MXenes	Methods	Application	Refs
Ti_3C_2Tx	Acid (HCl + LiF)	Direct absorption solar collectors	Li et al. (2020)
Ti_3C_2Tx	Acid	Heterogeneous catalysts	Zeng et al. (2021)
	HF		
Ti_3C_2Tx	Acid (HCl + LiF)	Flexible Supercapacitors	Sun et al. (2021)
Ti_3C_2Tx	Acid (HCl + LiF)	Adsorption	Ihsanullah and Ali, (2020)
Ti_3C_2Tx	Acid (HCl + LiF)	Adsorption	Khan et al. (2019)
Ti_3C_2	Acid (NH_4HF_2)	electrocatalyst	Abdullah et al. (2020)
Ti_3C_2Tx	Acid	Gas barrier nanocomposite films	Woo et al. (2020)
	HF		
Ti_3C_2	Acid (NH_4HF_2)	Energy storage properties and thermal conductivity	Aslfattahi et al. (2020)
Ti_2NTx	Acid	Biological activity	Szuplewska et al. (2019b)
	HF		
V_2CTx	Acid	Aluminum Batteries	VahidMohammadi et al. (2017)
	HF		
Ti_2N	Acid	Surface-Enhanced Raman Scattering Substrate	Soundiraraju and George, (2017)
	HF		
Ti_3C_2Tx	NH_3F	supercapacitors	Wang et al. (2016)
Zr_3C_2Tx	Acid	Electrical energy storage	Zhou et al. (2016)
	HF		
Ti_3C_2Tx	Acid (HCl + LiF)	Electrochemical sensor	Wang et al. (2021c)
Ti_3C_2Tx	NaOH	—	Li et al. (2018)
Ti_4N_3	Molten salts	—	Urbankowski et al. (2016)
$(Mo_2Ti_2)C_3Tx$	TBAOH + HF	Thermoelectricity	Anasori et al. (2016)

$M_{n+1}X_nT_x$, whereas M refers to Mn, V, Cr, Hf, Ti, Nb, Zr, Sc, Wd etc., N or C; n is one or two; Tx refers to oxygen, hydroxyl, or fluorine MXenes be prepared by etching (Cd, Ga, Si, As, Al, Ge, In, Ti, and Sn elements) layers of MAX phase. Figure 1A of the periodic table shows that using the ingredients of MAX phases, $M_{n+1}AX_n$ (MAX) phases are usually the starting compounds. As shown in Figure 1B, MXenens are formed by exfoliating in the A (Cd or Al) layers (Guo et al., 2016; Wang et al., 2018; Hart et al., 2019).

In general, there are two methods for synthesizing 2D substances. The bottom-up is the first method. For example, CVD (chemical vapor deposition) would generate great definition films in different layers. This way is not commonly used to synthesize MXenes, since the resulting films are not a single layer. Xu et al. (2015) utilized the CVD method to make Molybdenum carbide (Mo_2C), Tungsten carbide, and Tantalum carbide thin films. However, even the thinnest Mo_2C films had a minimum of six Mo_2C layers and not single MXenes sheets. The second method is a top-down method that involves peeling off layered solids. The second method would be classified into two types mechanical and chemical peels.

For instance, an adhesive can use an adhesive strip to detach graphene layers (Novoselov et al., 2004). This method is not appropriate for MAX phases because, compared to another three-dimensional solid utilized as precursors to their two-dimensional similar, the bonds among M -Al are, in Most cases, metallic/covalent. Most MAX steps based on Al are synthesized to above T = 1,300°C (Barsoum, 2013). This approach is not applicable here. The remarkable point is that before the discovery of MXene, it was thought that only weakly bonded three-dimensional layered solids could be delaminated. Therefore, the top-down method converts three-dimensional to two-dimensional solids by chemical peeling by weakening the interlayer bonds. One way is to bond the layers together to be easily dispersed in a solvent (Nicolosi et al., 2013). Therefore, the vital issue is to find the right combination of intercalant and solvent. Chemical etching is the first method to synthesize Mxenes from MAX phases (bonded solids) (Naguib et al., 2011b; Li et al., 2015). At the moment, various types of ternary carbide and MAX nitride have been mentioned, which make a significant difference to this family. According to theoretical predictions, more than thirty types of MXenes have been tested; more are expected to be used (Pan et al., 2017; Frey et al., 2019). The various MXene acquired to date have been synthesized using different methods, precursors, etching methods, and bright lights (Garg et al., 2020).

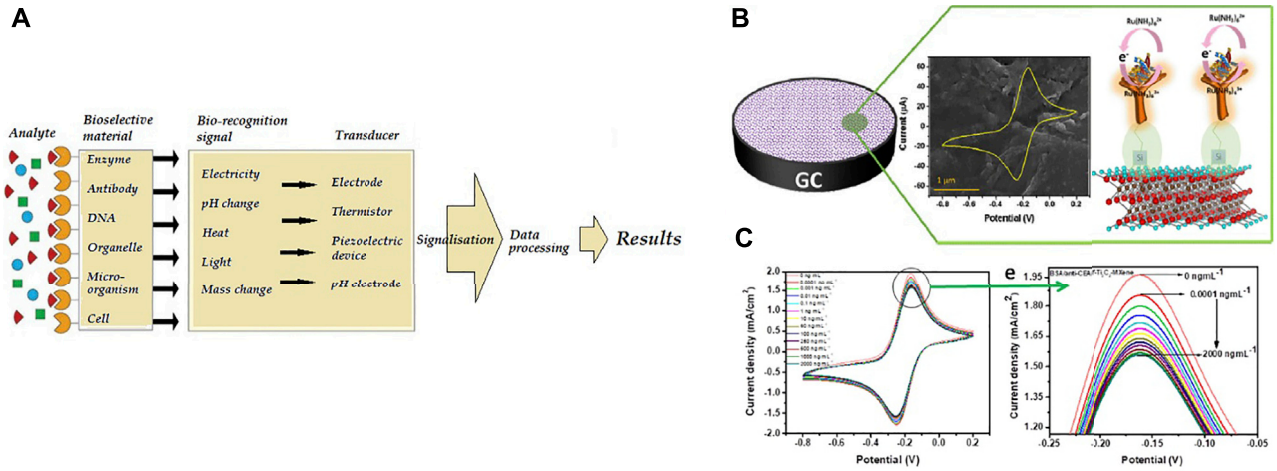

FIGURE 2
(A) The biosensor processes principle (Kivirand et al., 2013) **(B)**Schematic of the electrochemical biosensor (BSA/anti-CEA/f-Ti_3C_2-MXene/GCE) for CEA diagnosis, **(C)** diagram of electrochemical biosensor replies at various concentrations of CEA (Kumar et al., 2018).

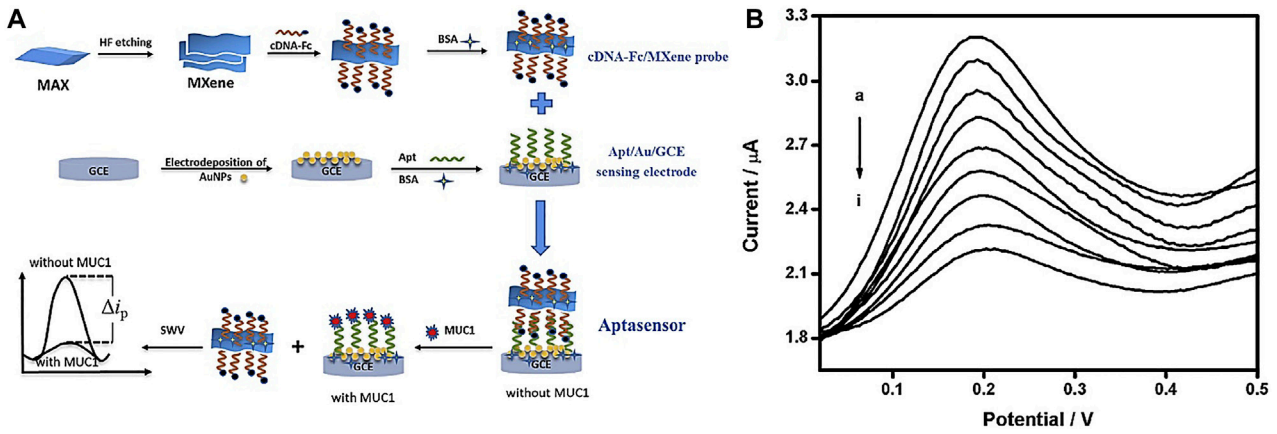

FIGURE 3
(A) Schematic of competitive aptasensor manufacturing and detection method, **(B)** diagram of electrochemical biosensor replies at various concentrations of MUC1 (Wang et al., 2020).

Precursors, MAX phases form a big family of 130 or more combinations, most of which are crystallized in the space group P63/mmc, or derived. This structure is combined with MX6 octagonal combined with net layers of A. The principal variation between the three types (n is one, two, or three) of the MAX phase is the number of layers M (2–4) between layers A.

In the formation of MXene from MAX, etched layers are replaced by various groups of Tx like fluorine and oxygen. After the etching process, the material is composed of $M_{n+1}X_nT_x$ in several layers, the bond between which is hydrogen and Vander Waals (Verger et al., 2019).

Exfoliation is after the etching stage. Exfoliation hinges on the etching methods and the position of the MXene. Removed by-products (such as Aluminum fluoride), the resulting layers were rinsed multiple times with water after the etching process. The acid may be utilized for pre-washing with H_2SO_4 or hydrochloric acid as a salt dissolving aid (aluminum fluoride or lithium fluoride). Only then can the layers be exfoliated to form colloidal suspensions containing several or more layers of MXene (Naguib et al., 2011b; Ghidiu et al., 2016; Urbankowski et al., 2016). Table 1 summarizes the different types of MXene synthesized methods.

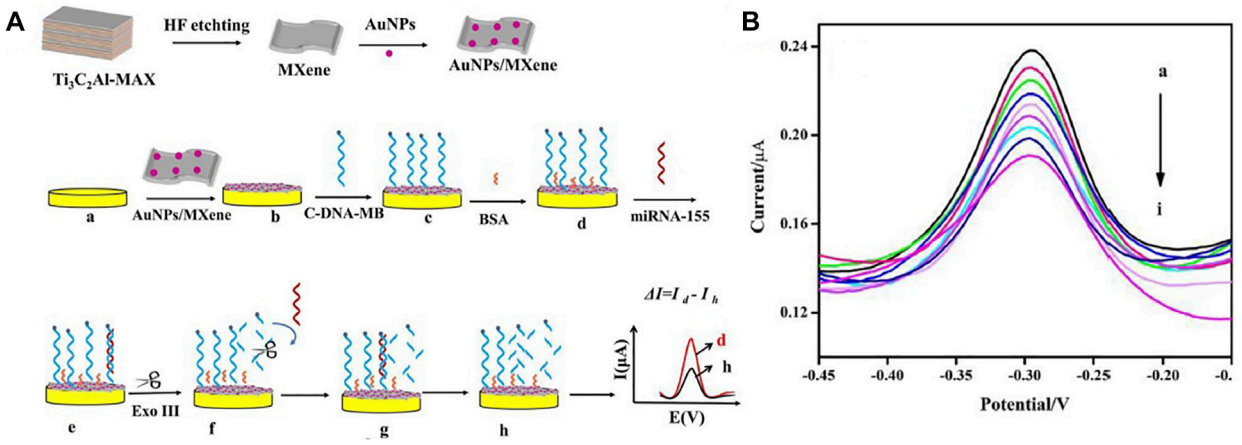

FIGURE 4
(A) Schematic of manufacturing electrochemical biosensor based Au/MXene to diagnosis miRNA-155, **(B)** diagram of electrochemical biosensor replies at various concentrations of miRNA-155 (linear range from 1.0 fM –10 nm) (Yang et al., 2020).

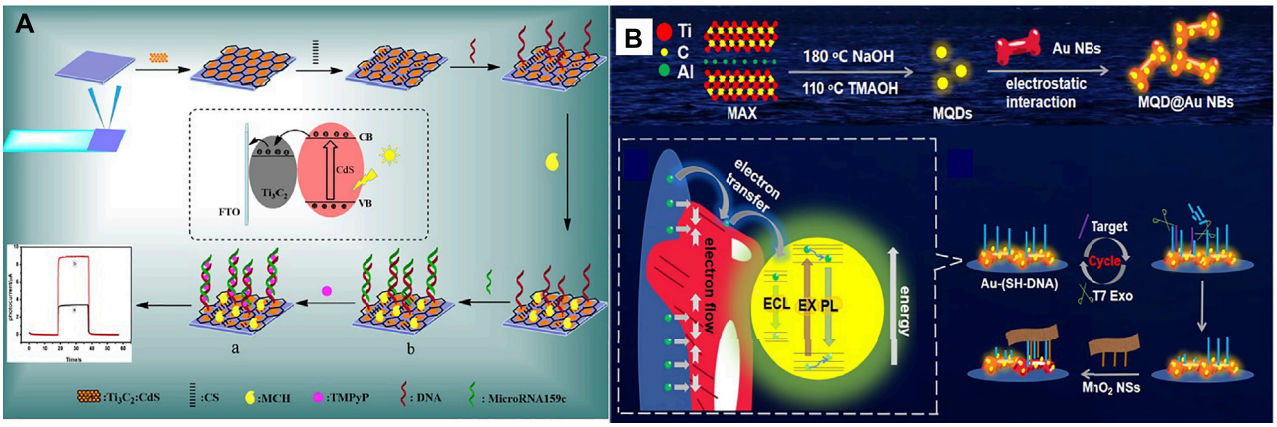

FIGURE 5
(A) Schematic of manufacturing photoelectrochemical biosensor based a Ti_3C_2:CdS to detect miRNA159c (Liu S.-T. et al., 2020), **(B)** Schematic of manufacturing ECL biosensor based on MQD/Au to detect miRNA-26a (Nie et al., 2021).

3 Biosensors for breast cancer diagnosis

As previously mentioned in the first part of this article, various diagnosis methods of breast cancer based on Mxene were surveyed. Also, the advantage and limitations of these materials were investigated. In summary, ultrasound imaging, ELISA, IHC, and mammography are usually utilized for breast cancer detection and monitoring its advance (Ali et al., 2015). Nevertheless, each one of these diagnostic methods faces constraints such as specimen pretreatment, the need for expensive equipment, time-consuming, etc. Thus, it is expected to use novel, sensitive, rapid, and less aggressive methods such as biosensors to detect breast cancer (Dervisevic et al., 2020; Wang Z. et al., 2021).

Each biosensor is applicably comprised of three parts. The first section of the biosensor is the biological component that is reliable for analyte detection and causing the answer signal. The signal caused is then converted, which is reliable for analyte detection and causing the answer signal. The signal caused is then converted into a recognizable response by a second part called a transducer, the most vital part of any biosensor system. The third section is the biosensor detector,

TABLE 2 The types of MXene-based biosensors for detecting breast cancer.

Target	Nanoparticle	Type of biosensor	Linear range/LOD	Refs
miRNA-26a	MQD@Gold	Electrochemiluminescence	Linear range = 5 fM to 10 nM LOD = 1.7 fM	Nie et al. (2021)
MUC1	MXene/Au	Electrochemical aptasensor	Linear range = 1.0 pM–10 μM LOD = 0.33 p.m.	Wang et al. (2020)
miRNA-155	AuNPs/Ti_3C_2 MXene	Electrochemical biosensor	linear range = 1.0 fM to 10 nM LOD = 0.35 fM	Yang et al. (2020)
CEA	Ti_3C_2-MXene	Electrochemical biosensor	Linear range = 0.0001–2000 ng ml^{-1} LOD = 0.000018 ng ml^{-1}	Kumar et al. (2018)
microRNA159c	Ti_3C_2:CdS	Photoelectrochemical biosensor	Linear range = 1.0* 10^{-6}–1.0 * 10^{-13} mol L^{-1} LOD = 33 fmol L^{-1}	Liu et al. (2020a)

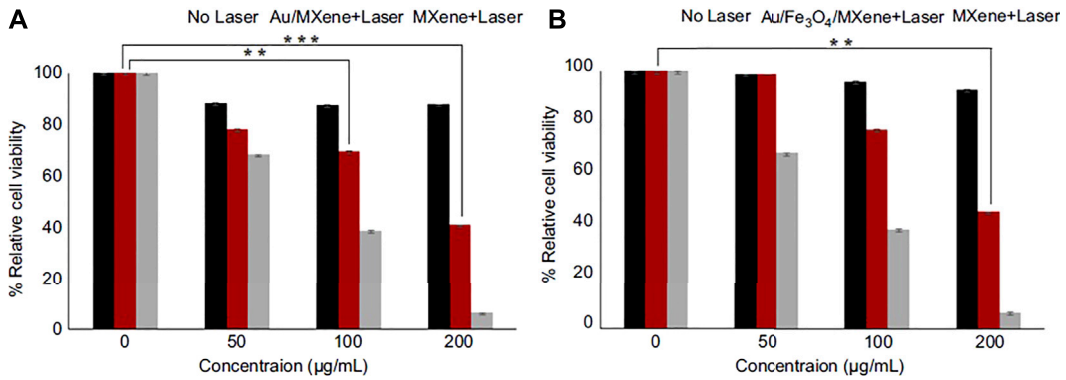

FIGURE 6
The relative viability of MCF7 cells since incubation (various concentrations) **(A)** Au/MXene and **(B)** Au/Fe_3O_4/MXene and Ti_3C_2 (MXene) following by NIR 808 nm laser radiance with a might density of 1.0 W/cm^2 for 5 min Standardized to control (without laser treated cells) (Hussein et al., 2019).

which processes and amplifies the signals before display utilizing an electronic display technique (Kivirand et al., 2013; Parkhey and Mohan, 2019). The different stages in signal processing of a biosensor, from measurement to transmission to display, are illustrated in Figure 2A.

Biosensors could be organized by conforming to the bio-identification element or physiochemical transfer type. Biosensors could be classed as piezoelectric, electrochemical, thermal and optical biosensors based on the converter (Pejcic et al., 2006; Darroudi et al., 2022; Hatamluyi et al., 2022).

Among biosensor types, Electrochemical biosensors are the widest biosensors studied because they have the boon of low detection limit, the plainness of construction, specificity, and comfort of the procedure. With recent boons in electronic tools, the biosensors cloud be used as on-chip laboratory instruments for *in-vivo* monitoring or as a handheld technology for on-site miniature (Ronkainen et al., 2010; Sawant, 2017).

3.1 MXene-based biosensors

Kumar et al. (2018) designed an unlabeled and high-sensitivity electrochemical biosensor for carcinoembryonic antigen (CEA) diagnosis based on Ti_3C_2 nanosheets. Then Ti_3C_2 nanosheets were functionalized with APTES for anti-CEA covalent stabilization. Figure2B shows A schematic of the electrode surface and the redox probe interplay. The designed biosensor (BSA/anti-CEA/f-Ti_3C_2-MXene/GCE) shows a wide detection range of 0.0001–2000 ng ml^{-1} (Figure 2C) with LOD 0.000018 ng ml^{-1}.

In another study, Wang et al. (2020) developed a competitive electrochemical biosensor-based cDNA-Fc/MXene probe to detect the MUC1 (Mucin1) as a breast cancer marker. MUC1 is a transmembrane glycoprotein, which is attention due to its unnormal expression in tumor tissues (people patients) for detection (Li et al., 2019). MXene was used as a nanobearer for cDNA-Fc to strengthen diagnosis signals and provided wide connection

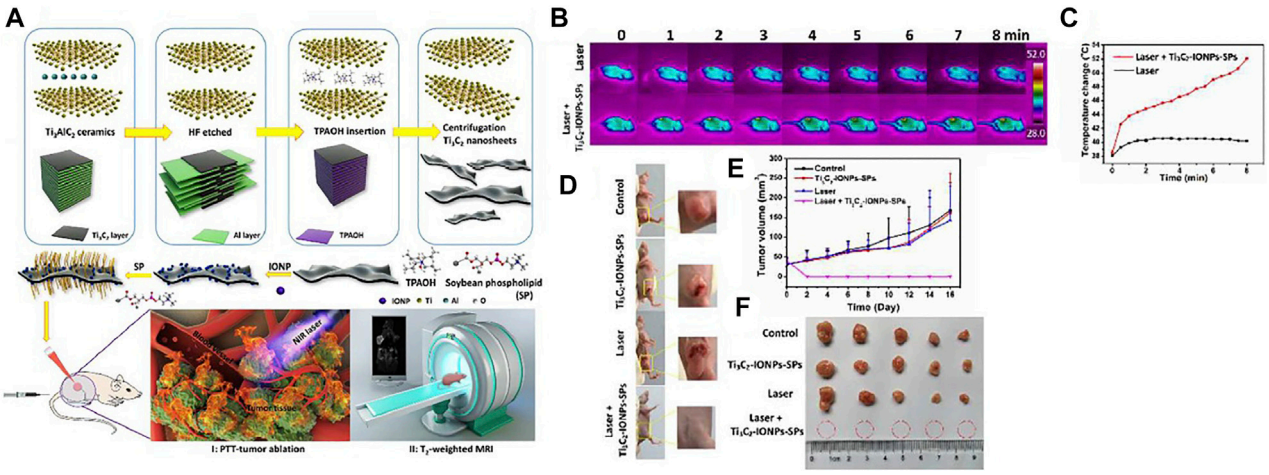

FIGURE 7
(A) Schematic of Ti_3C_2-IONPs-SPs synthesis and their multiple functions for tumor theranostics, **(B)** IR thermographic photographs of cancer mice afore and behind infusion of Ti_3C_2-IONPs-SPs nanocomposite followed by NIR radiance, **(C)** the temperature rise of tumors within the NIR radiance flow, **(D)** Digital images of mice with 4T1 tumor on the 16th day behind PTT therapies, **(E)** Tumor volume change plots of different groups of mice carriers of the tumor behind various therapies. **(F)** Collected digital images of tumors for every group at the PTT therapy end (Liu et al., 2018b).

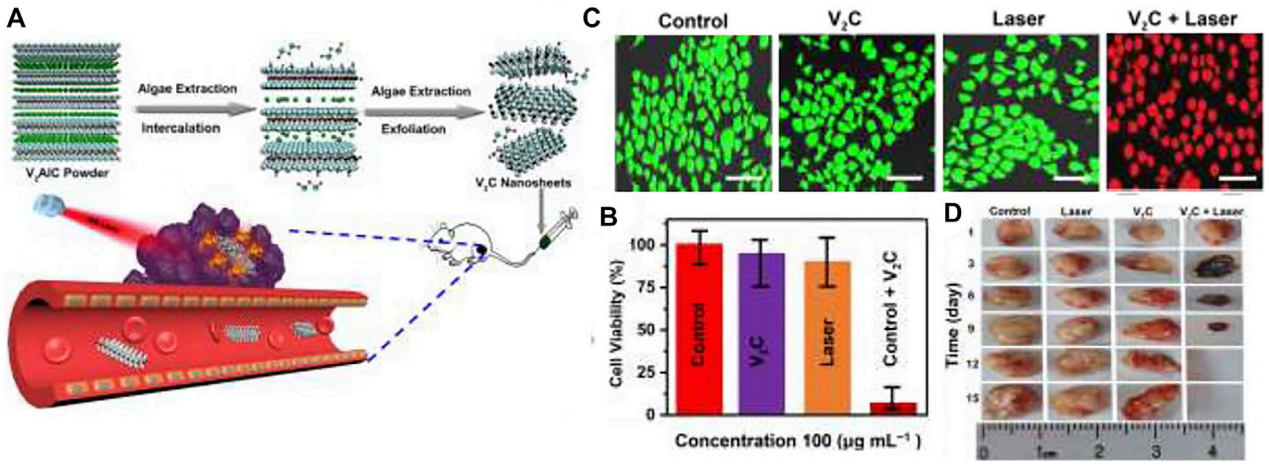

FIGURE 8
(A) Schematic representation of V_2C-NSs synthesis and usages for PTT, **(B)** MTT method, and **(C)** result of Calcein AM/PI dual coloring of MCF-7 cell livability remedied with different treatment groups, **(D)** Tumor size photograph (Zada et al., 2020).

locations for cDNA-Fc binding. Figure 3A shows that detection involves three operations: linking the cDNA-Fc over MXene, bonding between Apt over the Au/GCE, and competitive detection of MUC1. To detect MUC1, the cDNA-Fc/MXene probe binds with Apt/Au/GCE and forms the aptasensor cDNA-Fc/MXene/Apt/Au/GCE. next stage; the aptasensor was registered in phosphate buffer solution as the primary signal. When the aptasensor is utilized to detect MUC1, the competitive approach begins. The MUC1 vies with cDNA-Fc/MXene probe for connecting the Apt/Au/GCE. Linking of MUC1 to aptamer causes a change in DNA composition, forcing the previously formed Apt/cDNA-Fc double strand to disintegrate and the cDNA-Fc/MXene probe detached from the biosensor, reducing the signal. The designed electrochemical aptasensor offers a large linear range from 1.0 p.m. to 10 μM (Figure 3B) and a LOD of 0.33 p.m., which is a bright idea in clinical detection.

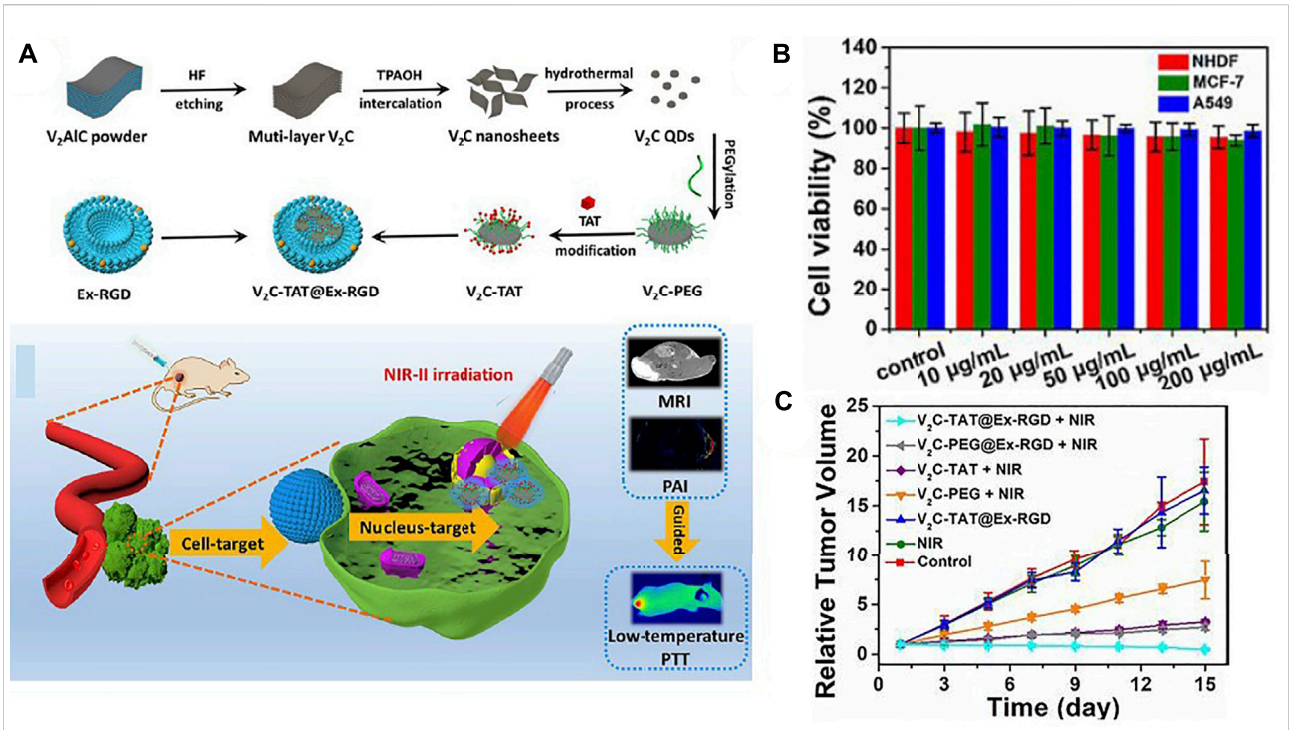

FIGURE 9
(A) The V_2C-TAT@Ex-RGD preparation process and schematic of nuclear organ and cancer cell membrane with the dual objective of V_2C-TAT@Ex-RGD nano-agent for PTT. **(B)** Check Cell viability of different cells (MCF-7, A549, and NHDF cells) were incubated at various concentrations V_2C-TAT@Ex-RGD, **(C)** relative tumor growth plots in multiple groups (Cao et al., 2019).

Interestingly, Yang et al. (2020) developed an electrochemical biosensor (cDNA/AuNPs/MXene) for mir-155 diagnosis by cascading target recovery using exonuclease III (Figure 4A). The biosensor 3D structure of the AuNPs/Ti3C2 enjoys significant electrical conductance, wide integrated surface area, and electrocatalytic attributes. Au nanoparticles are utilized to stabilize adsorbed cDNA by Au-S chemical bonding. The cDNA was bonded together with MB then the primitive DPV signal was recorded (Id). Next, cDNA and miRNA-155 were connected. Then exonuclease III recapitulated the end of the 3 ′cDNA in a double-stranded format, causing a reduced electrochemical signal (Ih). The designed electrochemical biosensor achieved a wide linear range from 1.0 fM -10 nm (Figure 4B) and a LOD of 0.35 fM. It also shows reproducibility, stability, and desirable characteristics.

In another study, Liu et al. (2020) designed a photoelectrochemical biosensor based on a Ti_3C_2:CdS to detect miRNA159c (Figure 5A). Nanocomposites of CdS: Ti_3C_2 were utilized as materials of optoelectronic, which remarkably improved the photoelectric transformation yield. The linear range of miRNA159c was 1.0×10^{-6} to 1.0×10^{-13} mol L^{-1}, and the LOD of 33 fmol L^{-1}. The designed biosensor provided an adequate diagnosis for breast cancer. Also, Nie et al. (2021) manufactured an Electrochemiluminescence biosensor based on MXene-quantum dot (MQD) and gold-nano bone detection of miRNA-26a, as shown in Figure 5B. The green procedure synthesized MQDs. MQDs and gold NBs with unparalleled electrochemical effects significantly increased electrochemiluminescence with conductivity and SPR properties. As a result, the diagnosis concentration was wide-ranging from 5 fM-10 nm and the LOD was 1.7 fM. This biosensor has been used successfully to diagnose serum samples from patients of clinical.

As can be seen, all studies with a variety of biomarkers for detecting breast cancer using MXene showed a better detection limit and range. In the following, the detection range and limit of detection of different types of MXene-based biosensors for breast cancer diagnosis have been brought in Table 2.

4 Systemic therapy considerations

Breast cancer is mainly removed via surgery with radiation therapy or chemotherapy (Nounou et al., 2015). Though these are the most practical therapies, they are by an imperfect delete of tumor via surgery that can conduce to tumor relapse (Tohme et al., 2017). In addition, radiation therapy and chemotherapy have multiple side effects such as problems of intestinal, harm to healthy tissues, nausea, and loss of hair (Hussein et al., 2019). Photothermal therapy (PTT) is a non-invasive treatment of cancer that

TABLE 3 Investigated biocompatibility, photothermal conversion efficiency, and the effect of MXene nanoplate cell ablation on different types of breast cancer cells.

Composition	Wavelength	Photothermal conversion efficiency	Cell line	Result/biocompatibility	Strategy	Refs
Au/MXene Au/Fe_3O_4/MXene	NIR-I (Laser 808 nm, 1W/cm^2)	—	MCF-7	*In-vivo* cytotoxicity measure utilizing zebrafish fetal displayed that Au/Fe_3O_4/MXene and AU/MXene had lower fetal murrain (LC» 1,000 μg/ml) than only MXene (LC = 257.46 μg/ml). Also, no apparent toxicity was observed for "without-Laser" indicating great bio-compatibility of nanocomposites	PTT	Hussein et al. (2019)
Ti_3C_2-IONPs-SPs	NIR-I (Laser 808 nm, 1.5W/cm^2)	48.6%	4T1	Ti_3C_2-IONPs-SPs have significant photothermal conversion efficiencies (48.6%) to decrease tumor tissues and kill cancer cells *in-vitro* and *in vivo* conditions For Nanocomposite (Laser-free), no displayed cytotoxicity was observed	PTT	Liu et al. (2018b)
V_2C-TAT@ Ex-RGD	NIR-II (Laser 1,064 nm, 0.96W/cm^2)	45.05%	MCF-7	Cell viability (>90%) for The V_2C-TAT@Ex-RGD in different cells (MCF-7, NHDF and A549, *in vitro*) The V_2C-TAT@Ex-RGD + Laser group showed substantial and effective suppression of tumor growth, and no recurrence occurred (*in-vivo* method)	PTT	Cao et al. (2019)
V_2C-NSs	NIR-I (Laser 808 nm, 0.48 W/cm^2)	48%	MCF-7	Low toxicity in *in-vitro* method, V_2C-NSs + Laser murdered approximately all cells (*in-vivo*)	PTT	Zada et al. (2020)
Nb_2C-MSNs-SNO	NIR-II (Laser 1,064 nm, 1.5 W/cm^2)	39.09%	HUVEC, 4T1	There is slight cytotoxicity to HUVEC and 4T1 cells, No chronic or acute response *in-vivo*. Optimal expulsion conduct, Nb_2C-MSNs-SNO + Laser reduce tumor growth (*in-vivo*)	PTT	Yin et al. (2020)
Ti_3C_2-SPs	NIR-I (Laser 808 nm, 1W/cm^2)	74.6%	4T1	#0D0D0D; Ti_3C_2 is a drug delivery (DOX) nano-platform for effective chemotherapy with great photothermal transformation ability of Ti_3C_2 for tumor deracination by photothermal ablation (both *in-vivo* and *in-vitro*), with No chronic or acute response *in-vivo*. Optimal expulsion conduct	PTT/ chemotherapy	Han et al. (2018)
Ti_2C-PEG	NIR-I (Laser 808 nm)	87.1%	MCF-7 non-malign MCF-10A	Fine bio-compatibility *in-vitro*, favorably effective cancer cell erosion, and well selectivity than malign cells	PTT/ Photodynamic	Szuplewska et al. (2019a)
Nb_2C-PVP	NIR-I (Laser 750–1,000 nm, 1W/cm^2) and NIR-II (Laser 1,000–1,350 nm, 1W/cm^2)	NIR-I = 36.4% NIR-II = 45.65%	4T1	Nb_2-PVP has little cytotoxicity (*in-vitro*) and great bio-compatibility PPT ablation and tumor deracination (performance effective in both NIR-II and NIR-I, *in-vivo*)	PTT	Lin et al. (2017)
HAP/CS/HA/ MXene HAP/CS/HA/ MXene/AuNRs	NIR-I (Laser 808 nm, 2 W/cm^2)	HAP/CS/HA/ MXene = 13.76% HAP/CS/HA/MXene/ AuNRs = 20.42%	MCF-7	Nanoplatforms have good bio-compatibility (*in-vitro*) and good photothermal transformation yields (*in-vivo*) with excellent potential for remote drug delivery (DOX)	PTT/drug delivery	Wu et al. (2021)
Ti_3C_2-CoNWs	NIR-I (Laser 808 nm, 2 W/cm^2)	34.42%	4T1	Ti_3C_2-CoNWs nanocarriers show great photothermal transformation efficiency under Laser radiance and excellent medicine loading capacity (DOX, 225.05%)	Chemo-PTT/ drug delivery	Liu et al. (2020b)

(Continued on following page)

TABLE 3 (*Continued*) Investigated biocompatibility, photothermal conversion efficiency, and the effect of MXene nanoplate cell ablation on different types of breast cancer cells.

Composition	Wavelength	Photothermal conversion efficiency	Cell line	Result/biocompatibility	Strategy	Refs
H-Ti_3C_2-PEG	NIR-II (Laser 1,064 nm, 1 W/cm^2)	Ti_3C_2 = 50.8% H-Ti_3C_2-PEG = 49.6%	4T1	Nanoplatforms have good biocompability and stability (*in-vitro* and *in-vivo*) and could improve the SDT performance It is important to note that H-Ti_3C_2-PEG is eliminated from the body. Furthermore, they arenot harmful long-term	PTT and SDT	Li et al. (2022)

murders tumor cells with heat and may altogether remove the tumor (Gong et al., 2020; Jiang et al., 2020; Wang et al., 2021b). Accordingly, it is more premier compared to removing surgically.

4.1 Biocompatibility and toxicity

Williams defined biocompatibility as the biomaterial's ability to accomplish its intended function concerning medical treatment without causing any local or systemic adverse on the receptor or beneficiary of that treatment, but the most appropriate helpful tissue or cellular reply in that particular situation and optimizing the clinically related performance of that treatment (Williams, 2008). Biomaterial biocompatibility is fundamental system property emanated from medical, physical, biological, chemical, and design elements (Ahmed et al., 2012).

Therefore, materials of biocompatible requirements to have the feature such as suitable mechanical loading necessary; capacity for long-time storage, against chemical assault resistance by physiological fluids, resistance to corrosion, suitable density, not cause allergic or immunologic responses, and no poisonous or carcinogenic; etc. Toxicological effects of NPs relate to their ability to adversely affect human or animal physiology or directly interfere with organ and tissue function. The overall shape, particle size, surface charge, stability, and composition of NPs, all play a role in toxicity. As these nanoparticles are used in biomedical applications, they will be directly in contact with tissues and cells, making their biocompatibility a vital issue (Li et al., 2012).

The next part examines the photothermal property, biocompatibility, and toxicity of MXene nanoparticles in terms of compatibility, tissue compatibility, and cytotoxicity.

4.2 Photothermal therapy

MXene has a photothermal efficacy, meaning that it could transform the energy of Laser- light into the power of heat by intensifying the surface plasmon efficacy. Thus, scientists have researched MXenes for the PTT of cancer, who used in the murdering of cancer tumors via heat, which leads to denaturation of protein and, finally, cell death (Liu et al., 2017; Liu et al., 2018a; Wang and Cheng, 2019). MXenes with a size of about 180 nm could attain the cancerous microenvironment via increasing permeance and maintaining EPR (Gazzi et al., 2019).

For example, Hussein and colleagues (Hussein et al., 2019) designed plasmonic-based nanocomposites Au/Fe_3O_4/Ti_3C_2 and Au/Ti_3C_2 with anticancer PTT (photothermal therapy) treatment abilities that lesser *in-vivo* toxicity than Ti_3C_2. The photothermal transformation capability of Au/Fe_3O_4/MXene and Au/MXene at the cellular level was assessed utilizing the cell line of breast cancer (MCF7). Behind incubation (with various concentrations of nanocomposites), evaluated the comparative viability of the cell without and with laser exposure. No apparent cytotoxicity was seen for "laser-free," showing the high biocompatibility of nanocomposites (Figure figure6A). Also, Nanocomposites were subjected to a NIR laser (808 nm, 1.0 W/cm^2) to assess the photothermal transformation performance for 5 min. According to Figure 6B, cell livability gradually reduced with the gaining concentration of both nanocomposites. Therefore, new nanocomposites can be more suitable and safer than Ti_3C_2 for biomedical applications, especially in the PTT method.

In another study, Liu et al. (2018b) used magnetic MXenes for effective cancer therapy. The MXene is used by increased photothermal transformation ability for effective PTT versus cancer and IONPs action as a contrast factor for T_2-weight MRI. Figure 7A displays synthesizing Ti_3C_2-IONPs nanocomposite and their particular theranostic function for cancer therapy. For the increased biocompatibility and stability of MXene-IONPs under physiological conditions, soybean phospholipids (Ti_3C_2-IONPs-SPs) were used. After Ti_3C_2-IONPs-SPs intravenous Injection, the tumor was irradiated straightly under the NIR laser (1.5 Wcm^{-2},

808 nm for 8 min). The tumor temperature variation was scanned via an IR thermal imaging camera monitored. Figures 7B,C displayed that the laser + Ti_3C_2-IONPs-SPs group temperature rose rapidly after NIR Laser radiance. But the Laser group temperature rose by only 2°C. The tumor disappeared considerably, and a black scar remained on the main sites of the tumor for the first days. However, other tumor groups constantly grew over a 16-days study period (Figures 7D–F). As a result, this nanocomposite Ti_3C_2-IONPs show high T_2 relaxation of 394.2 $mM^{-1}s^{-1}$ and MRI with efficient tumor contrast, which provides the potential to conduct PTT. Ti_3C_2-IONPs have significant photothermal conversion efficiencies (48.6%) to decrease tumor tissue and kill cancer cells *in vitro* and *in vivo* (BALB/c nude and Kunming mice).

V_2C (vanadium carbide) has well potential in the PTT method. Nevertheless, the usage of V_2C in PTT is restricted due to difficult synthesis conditions and low PTCE. Zada and colleagues (Zada et al., 2020) developed a green synthesis way utilizing the extraction of algae to make V_2C NSs for positively effectual *in-vivo* and *in-vitro* tumors photothermal ablation (Figure 8A). They investigated the effect of photothermal and bio-compatibility of V_2C-NSs and anticancer function *in-vitro* on MCF-7 cells. Figure 8B shows that the V_2C-NSs and Laser of NIR (0.48 W/cm, 808 nm, 10 min) alone showed partial toxicity. In contrast, V_2C-NSs + Laser displayed considerable anticancer agents and murdered approximately all cells. Calcein AM/PI dual coloring analysis was compliance cum MTT outcomes (Figure 8C). These outcomes showed well *in vitro* anticancer efficacy of V_2C-NSs owing to enhanced photothermal effectiveness. To check the anticancer efficacy of *in-vivo* studies, nude mice carrying MCF-7 tumors were separated into the control group (only PBS treatment), the Laser group, the V_2C-NSs inject group, and the laser + V_2C-NSs group. Laser + V_2C-NSs combined therapy was considerably more efficacious in inhibiting tumor growth than the other groups. Finally, the tumor disappeared after 12 days (Figure 8D). Results demonstrated the excellent anticancer efficiency of V_2C-NSs *in vivo*.

The finite influence deepness of PTAs active in the NIR-I bio-window and thermal resistance induced by HSP considerably restrict the remedial effect of PTT. To solve this issue, Cao et al. (2019) introduced a PTT strategy for targeting (at down-temperature) nuclei in the NIR-II area that combines quantum dots of vanadium carbide (V_2C-QDs) of PTA and Ex vector to kill effective tumors. Figure 9A shows the synthesis of V_2C-QDs modified with Ex and TAT peptides (V_2C-TAT@EX-RGD) with good thermal efficacy in the NIR-II region for PTT and good ability for MRI, fluorescent and photoacoustic imaging. The V_2C-TAT@Ex-RGD *in vitro* cytotoxicity in different cells (MCF-7, NHDF, and A549) was evaluated using the MTT method. Figure 9B shows that V_2C-TAT@Ex-RGD displayed partial toxicity to all cell lines, and cell viability was upper 90%. High bio-compatibility, excellent transmission performance, etc., make V_2C-TAT@Ex-RGD an okay factor for PTT cancer. Seven groups were examined and displayed the plots of tumor growth (MCF-7 tumor) in Figure 9C. The group of control, V_2C-TAT@Ex-RGD intinction, and Laser (1,064 nm, 0.96W/$cm^{2,}$ and at 10 min) group have small suppressive efficacy upon tumor growth. V_2C-PEG + Laser group, V_2C-PEG@RGD + Laser, and V_2C-TAT + Laser have little tumor growth. Notably, the V_2C-TAT@Ex-RGD + Laser group showed substantial and effective suppression of tumor growth, and no recurrence occurred.

In Table 3, biocompatibility, photothermal conversion efficiency, and MXene nanosheet cell ablation effects on different types of breast cancer cells were investigated.

Due to the particular specifications of MXenes, these attractive features are crucial for their usages, such as biomedical (photothermal), antimicrobial use, and biosensors. Investigators have constructed prominent endeavors to develop synthesis and surface modification methods for diagnosis and treatment with photothermal for breast cancer. Detection and photothermal applications of MXenes are listed in Tables 2, 3 with surface profiles, limited detection, optical attributes, and conversion efficiency.

5 Coming prospects

The two-dimensional Mxene nanostructures are described in this study. But the rapid development of synthesized types of MXenes and their promising options for biomedical usage should be considered. Nanoplatforms based MXene on the response of small functional biomolecular, temperature, pH, and response should also be studied for probes and sagacious drug delivery so that diagnosis and effective therapy with fewer side effects can be achieved. Demonstrates a broad range of MXenes applications in the theragnostic of cancer, drug delivery, biosensors, and antimicrobial action that MXenes in early biomedical research may be believed to reduce or improve breast cancer.

6 Conclusion

This study provides an overview of the nanostructure of two-dimensional Mxene. It investigates different synthesis methods for producing biocompatible Mxenes and their application to the detection and therapy of breast cancer. In synthesis methods, a vast number of MXenes families are expected, while more recently, experimental species have been little demonstrated.

MXenes' surface modification is not only biocompatible but also has multifunctional properties, such as aiming ligands for preferential agglomeration at tumor sites for photothermal treatment that by the noncovalent reactions on the MXene surface with PEG, CS, SP, and PVP materials. The synthesized MXenes could modify to increase biodegradability/biocompatibility and decrease the cytotoxicity for particular biomedical usages. MXenes have a fantastic special for a great surface-to-volume proportion, antimicrobial attributes, drug delivery, engineering of tissue, and extensive near-infrared sorption. These features construct Mxenes as the most applicable materials for biological usage.

Author contributions

SR: Writing original draft, visualization, analysis data MD: Visualization, writing—review; editing BH: Writing—review; editing RA: Writing—review; editing SA-B: Writing—review; Editing MR: Writing—review; editing, supervision, MK: Writing—review; editing, supervision.

Conflict of interest

The authors declare that the research was conducted in the absence of any commercial or financial relationships that could be construed as a potential conflict of interest.

Publisher's note

All claims expressed in this article are solely those of the authors and do not necessarily represent those of their affiliated organizations, or those of the publisher, the editors and the reviewers. Any product that may be evaluated in this article, or claim that may be made by its manufacturer, is not guaranteed or endorsed by the publisher.

References

Abdullah, N., Saidur, R., Zainoodin, A. M., and Aslfattahi, N. (2020). Optimization of electrocatalyst performance of platinum–ruthenium induced with MXene by response surface methodology for clean energy application. *J. Clean. Prod.* 277, 123395. doi:10.1016/j.jclepro.2020.123395

Ahmed, M., Byrne, J., Keyes, T., Ahmed, W., Elhissi, A., Jackson, M., et al. (2012). "Characteristics and applications of titanium oxide as a biomaterial for medical implants," in *The design and manufacture of medical devices* (Elsevier), 1–57.

Ali, M. A., Mondal, K., Singh, C., Malhotra, B. D., and Sharma, A. (2015). Anti-epidermal growth factor receptor conjugated mesoporous zinc oxide nanofibers for breast cancer diagnostics. *Nanoscale* 7, 7234–7245. doi:10.1039/c5nr00194c

Anasori, B., Shi, C., Moon, E. J., Xie, Y., Voigt, C. A., Kent, P. R., et al. (2016). Control of electronic properties of 2D carbides (MXenes) by manipulating their transition metal layers. *Nanoscale Horiz.* 1, 227–234. doi:10.1039/c5nh00125k

Aslfattahi, N., Saidur, R., Arifutzzaman, A., Sadri, R., Bimbo, N., Sabri, M. F. M., et al. (2020). Experimental investigation of energy storage properties and thermal conductivity of a novel organic phase change material/MXene as A new class of nanocomposites. *J. Energy Storage* 27, 101115. doi:10.1016/j.est.2019.101115

Barsoum, M. W. (2013). *MAX phases: Properties of machinable ternary carbides and nitrides*. John Wiley & Sons.

Becker, S. (2015). *A historic and scientific review of breast cancer: The next global healthcare challenge*, 131, S36–S39.

Cao, Y., Wu, T., Zhang, K., Meng, X., Dai, W., Wang, D., et al. (2019). Engineered exosome-mediated near-infrared-II region V2C quantum dot delivery for nucleus-target low-temperature photothermal therapy. *ACS Nano* 13, 1499–1510. doi:10.1021/acsnano.8b07224

Darroudi, M., Ghasemi, K., Rezayi, M., and Khazaei, M. (2022). Toward early diagnosis of colorectal cancer: Focus on optical nano biosensors. *Mini Rev. Med. Chem.* 22. doi:10.2174/1389557522666220512142842

Darroudi, M., Gholami, M., Rezayi, M., and Khazaei, M. (2021). An overview and bibliometric analysis on the colorectal cancer therapy by magnetic functionalized nanoparticles for the responsive and targeted drug delivery. *J. Nanobiotechnology* 19 (1), 1–20. doi:10.1186/s12951-021-01150-6

Dervisevic, M., Alba, M., Prieto-Simon, B., and Voelcker, N. H. (2020). Skin in the diagnostics game: Wearable biosensor nano-and microsystems for medical diagnostics. *Nano Today* 30, 100828. doi:10.1016/j.nantod.2019.100828

Desantis, C. E., Ma, J., Gaudet, M. M., Newman, L. A., Miller, K. D., Goding Sauer, A., et al. (2019). Breast cancer statistics, 2019. *Ca. A Cancer J. Clin.* 69, 438–451. doi:10.3322/caac.21583

Frey, N. C., Wang, J., Vega Bellido, G. I. N., Anasori, B., Gogotsi, Y., and Shenoy, V. B. (2019). Prediction of synthesis of 2D metal carbides and nitrides (MXenes) and their precursors with positive and unlabeled machine learning. *ACS Nano* 13, 3031–3041. doi:10.1021/acsnano.8b08014

Garg, R., Agarwal, A., and Agarwal, M. (2020). A review on MXene for energy storage application: Effect of interlayer distance. *Mat. Res. Express* 7, 022001. doi:10.1088/2053-1591/ab750d

Gazzi, A., Fusco, L., Khan, A., Bedognetti, D., Zavan, B., Vitale, F., et al. (2019). Photodynamic therapy based on graphene and MXene in cancer theranostics. *Front. Bioeng. Biotechnol.* 7, 295. doi:10.3389/fbioe.2019.00295

George, S. M., and Kandasubramanian, B. (2020). Advancements in MXene-Polymer composites for various biomedical applications. *Ceram. Int.* 46, 8522–8535. doi:10.1016/j.ceramint.2019.12.257

Ghidiu, M., Halim, J., Kota, S., Bish, D., Gogotsi, Y., and Barsoum, M. W. (2016). Ion-exchange and cation solvation reactions in Ti3C2 MXene. *Chem. Mat.* 28, 3507–3514. doi:10.1021/acs.chemmater.6b01275

Gong, F., Cheng, L., Yang, N., Gong, Y., Ni, Y., Bai, S., et al. (2020). Preparation of TiH1. 924 nanodots by liquid-phase exfoliation for enhanced sonodynamic cancer therapy. *Nat. Commun.* 11, 1–11. doi:10.1038/s41467-020-17485-x

Guo, Z., Zhou, J., Zhu, L., and Sun, Z. (2016). MXene: A promising photocatalyst for water splitting. *J. Mat. Chem. A Mat.* 4, 11446–11452. doi:10.1039/c6ta04414j

Han, X., Huang, J., Lin, H., Wang, Z., Li, P., and Chen, Y. (2018). 2D ultrathin MXene-based drug-delivery nanoplatform for synergistic photothermal ablation and chemotherapy of cancer. *Adv. Healthc. Mat.* 7, 1701394. doi:10.1002/adhm.201701394

Hart, J. L., Hantanasirisakul, K., Lang, A. C., Anasori, B., Pinto, D., Pivak, Y., et al. (2019). Control of MXenes' electronic properties through termination and intercalation. *Nat. Commun.* 10, 1–10. doi:10.1038/s41467-018-08169-8

Hatamluyi, B., Rezayi, M., Jamehdar, S. A., Rizi, K. S., Mojarrad, M., Meshkat, Z., et al. (2022). Sensitive and specific clinically diagnosis of SARS-CoV-2 employing a novel biosensor based on boron nitride quantum dots/flower-like gold nanostructures signal amplification. *Biosens. Bioelectron. X.* 207, 114209. doi:10.1016/j.bios.2022.114209

Hussein, E. A., Zagho, M. M., Rizeq, B. R., Younes, N. N., Pintus, G., Mahmoud, K. A., et al. (2019). Plasmonic MXene-based nanocomposites exhibiting photothermal therapeutic effects with lower acute toxicity than pure MXene. *Int. J. Nanomedicine* 14, 4529–4539. doi:10.2147/ijn.s202208

Ihsanullah, I., and Ali, H. (2020). Technological challenges in the environmental applications of MXenes and future outlook. *Case Stud. Chem. Environ. Eng.* 2, 100034. doi:10.1016/j.cscee.2020.100034

Jastrzębska, A. M., Karwowska, E., Wojciechowski, T., Ziemkowska, W., Rozmysłowska, A., Chlubny, L., et al. (2019). The atomic structure of Ti2C and Ti3C2 MXenes is responsible for their antibacterial activity toward *E. coli* bacteria. *J. Mat. Eng. Perform.* 28, 1272–1277. doi:10.1007/s11665-018-3223-z

Jiang, J., Che, X., Qian, Y., Wang, L., Zhang, Y., and Wang, Z. (2020). Bismuth sulfide nanorods as efficient photothermal theragnosis agents for cancer treatment. *Front. Mat.* 7, 234. doi:10.3389/fmats.2020.00234

Karlsson, L. H., Birch, J., Halim, J., Barsoum, M. W., and Persson, P. O. (2015). Atomically resolved structural and chemical investigation of single MXene sheets. *Nano Lett.* 15, 4955–4960. doi:10.1021/acs.nanolett.5b00737

Khan, A. R., Husnain, S. M., Shahzad, F., Mujtaba-Ul-Hassan, S., Mehmood, M., Ahmad, J., et al. (2019). Two-dimensional transition metal carbide (Ti 3 C 2 T x) as an efficient adsorbent to remove cesium (Cs+). *Dalton Trans.* 48, 11803–11812. doi:10.1039/c9dt01965k

Kivirand, K., Kagan, M., and Rinken, T. (2013). Calibrating biosensors in flow-through set-ups: Studies with glucose Optrodes. *J State Art Biosensors-General Aspects*, 331–351.

Kumar, S., Lei, Y., Alshareef, N. H., Quevedo-Lopez, M., and Salama, K. N. (2018). Biofunctionalized two-dimensional Ti3C2 MXenes for ultrasensitive detection of cancer biomarker. *Biosens. Bioelectron. X.* 121, 243–249. doi:10.1016/j.bios.2018.08.076

Li, C., Zhang, M., Zhang, Z., Tang, J., and Zhang, B. (2019). Microcantilever aptasensor for detecting epithelial tumor marker Mucin 1 and diagnosing human breast carcinoma MCF-7 cells. *Sensors Actuators B Chem.* 297, 126759. doi:10.1016/j.snb.2019.126759

Li, G., Zhong, X., Wang, X., Gong, F., Lei, H., Zhou, Y., et al. (2022). Titanium carbide nanosheets with defect structure for photothermal-enhanced sonodynamic therapy. *Bioact. Mat.* 8, 409–419. doi:10.1016/j.bioactmat.2021.06.021

Li, T., Yao, L., Liu, Q., Gu, J., Luo, R., Li, J., et al. (2018). Fluorine-free synthesis of high-purity Ti $_3$ C $_2$ T $_x$ (T=OH, O) via alkali treatment. *Angew. Chem. Int. Ed.* 57, 6115–6119. doi:10.1002/anie.201800887

Li, X., Chang, H., Zeng, L., Huang, X., Li, Y., Li, R., et al. (2020). Numerical analysis of photothermal conversion performance of MXene nanofluid in direct absorption solar collectors. *Energy Convers. Manag.* 226, 113515. doi:10.1016/j.enconman.2020.113515

Li, X., Wang, L., Fan, Y., Feng, Q., and Cui, F. (2012). Biocompatibility and toxicity of nanoparticles and nanotubes. *J. Nanomater* 1–19.

Li, Z., Wang, L., Sun, D., Zhang, Y., Liu, B., Hu, Q., et al. (2015). Synthesis and thermal stability of two-dimensional carbide MXene Ti3C2. *Mater. Sci. Eng. B* 191, 33–40. doi:10.1016/j.mseb.2014.10.009

Lin, H., Chen, Y., and Shi, J. (2018). Insights into 2D MXenes for versatile biomedical applications: Current advances and challenges ahead. *Adv. Sci. (Weinh).* 5, 1800518. doi:10.1002/advs.201800518

Lin, H., Gao, S., Dai, C., Chen, Y., and Shi, J. (2017). A two-dimensional biodegradable niobium carbide (MXene) for photothermal tumor eradication in NIR-I and NIR-II biowindows. *J. Am. Chem. Soc.* 139, 16235–16247. doi:10.1021/jacs.7b07818

Liu, G., Zou, J., Tang, Q., Yang, X., Zhang, Y., Zhang, Q., et al. (2017). Surface modified Ti3C2 MXene nanosheets for tumor targeting photothermal/photodynamic/chemo synergistic therapy. *ACS Appl. Mat. Interfaces* 9, 40077–40086. doi:10.1021/acsami.7b13421

Liu, S.-T., Liu, X.-P., Chen, J.-S., Mao, C.-J., and Jin, B.-K. (2020a). Highly sensitive photoelectrochemical biosensor for microRNA159c detection based on a Ti3C2: CdS nanocomposite of breast cancer. *Biosens. Bioelectron. X.* 165, 112416. doi:10.1016/j.bios.2020.112416

Liu, Y., Han, Q., Yang, W., Gan, X., Yang, Y., Xie, K., et al. (2020b). Two-dimensional MXene/cobalt nanowire heterojunction for controlled drug delivery and chemo-photothermal therapy. *Mater. Sci. Eng. C* 116, 111212. doi:10.1016/j.msec.2020.111212

Liu, Z., Lin, H., Zhao, M., Dai, C., Zhang, S., Peng, W., et al. (2018a). 2D superparamagnetic tantalum carbide composite MXenes for efficient breast-cancer theranostics. *Theranostics* 8, 1648–1664. doi:10.7150/thno.23369

Liu, Z., Zhao, M., Lin, H., Dai, C., Ren, C., Zhang, S., et al. (2018b). 2D magnetic titanium carbide MXene for cancer theranostics. *J. Mat. Chem. B* 6, 3541–3548. doi:10.1039/c8tb00754c

Ma, Y., Jiang, K., Chen, H., Shi, Q., Liu, H., Zhong, X., et al. (2022). Liquid exfoliation of V8C7 nanodots as peroxidase-like nanozymes for photothermal-catalytic synergistic antibacterial treatment, S1742-7061(22)00370–00371. doi:10.1016/j.actbio.2022.06.031

Majeed, M. I., Bhatti, H. N., Nawaz, H., and Kashif, M. (2019). Nanobiotechnology: Applications of nanomaterials in biological research. *J. Integrating green Chem. Sustain. Eng.*, 581–615.

Mittal, S., Kaur, H., Gautam, N., and Mantha, A. K. (2017). Biosensors for breast cancer diagnosis: A review of bioreceptors, biotransducers and signal amplification strategies. *Biosens. Bioelectron. X.* 88, 217–231. doi:10.1016/j.bios.2016.08.028

Naguib, M., and Gogotsi, Y. (2015). Synthesis of two-dimensional materials by selective extraction. *Acc. Chem. Res.* 48, 128–135. doi:10.1021/ar500346b

Naguib, M., Kurtoglu, M., Presser, V., Lu, J., Niu, J., Heon, M., et al. (2011a). Two-dimensional nanocrystals produced by exfoliation of Ti3AlC2. *Adv. Mat.* 23, 4248–4253. doi:10.1002/adma.201102306

Naguib, M., Kurtoglu, M., Presser, V., Lu, J., Niu, J., Heon, M., et al. (2011b). Two-dimensional nanocrystals: Two-dimensional nanocrystals produced by exfoliation of Ti3AlC2 (adv. Mater. 37/2011). *Adv. Mat.* 23, 4207. doi:10.1002/adma.201190147

Naguib, M., Mochalin, V. N., Barsoum, M. W., and Gogotsi, Y. (2014). 25th anniversary article: MXenes: A new family of two-dimensional materials. *Adv. Mat.* 26, 992–1005. doi:10.1002/adma.201304138

Nazari, E., Arefnezhad, R., Tabadkani, M., Farzin, A. H., Tara, M., Hassanian, S. M., et al. (2021). Using correlation matrix for the investigation the interaction of genes and traditional risk factor in breast cancer. *Meta Gene* 30, 100947. doi:10.1016/j.mgene.2021.100947

Nicolosi, V., Chhowalla, M., Kanatzidis, M. G., Strano, M. S., and Coleman, J. N. (2013). Liquid exfoliation of layered materials. *Science* 340, 1226419. doi:10.1126/science.1226419

Nie, Y., Liang, Z., Wang, P., Ma, Q., and Su, X. (2021). MXene-Derived quantum dot@ gold nanobones heterostructure-based electrochemiluminescence sensor for triple-negative breast cancer diagnosis. *Anal. Chem.* 93, 17086–17093. doi:10.1021/acs.analchem.1c04184

Nounou, M. I., Elamrawy, F., Ahmed, N., Abdelraouf, K., Goda, S., and Syed-Sha-Qhattal, H. (2015). Breast cancer: Conventional diagnosis and treatment modalities and recent patents and technologies. Breast Cancer (Auckl). 9, S29420. doi:10.4137/bcbcr.s29420

Novoselov, K. S., Geim, A. K., Morozov, S. V., Jiang, D.-E., Zhang, Y., Dubonos, S. V., et al. (2004). Electric field effect in atomically thin carbon films. *Science* 306, 666–669. doi:10.1126/science.1102896

Pan, J., Lany, S., and Qi, Y. (2017). Computationally driven two-dimensional materials design: What is next? *ACS Nano* 11, 7560–7564. doi:10.1021/acsnano.7b04327

Pandey, R. P., Rasool, K., Madhavan, V. E., Aïssa, B., Gogotsi, Y., and Mahmoud, K. A. (2018). Ultrahigh-flux and fouling-resistant membranes based on layered silver/MXene (Ti 3 C 2 T x) nanosheets. *J. Mat. Chem. A Mat.* 6, 3522–3533. doi:10.1039/c7ta10888e

Parkhey, P., and Mohan, S. V. (2019). "Biosensing applications of microbial fuel cell: Approach toward miniaturization," in *Microbial electrochemical technology* (Elsevier), 977–997.

Pejcic, B., De Marco, R., and Parkinson, G. (2006). The role of biosensors in the detection of emerging infectious diseases. *Analyst* 131, 1079–1090. doi:10.1039/b603402k

Qi, B., Wang, C., Ding, J., and Tao, W. (2019). Editorial: Applications of nanobiotechnology in pharmacology. *Front. Pharmacol.* 10, 1451. doi:10.3389/fphar.2019.01451

Rasool, K., Helal, M., Ali, A., Ren, C. E., Gogotsi, Y., and Mahmoud, K. A. (2016). Antibacterial activity of $Ti_3C_2T_x$ MXene. *ACS Nano* 10, 3674–3684. doi:10.1021/acsnano.6b00181

Ronkainen, N. J., Halsall, H. B., and Heineman, W. (2010). Electrochemical biosensors. *Chem. Soc. Rev.* 39, 1747–1763. doi:10.1039/b714449k

Salata, O. V. (2004). Applications of nanoparticles in biology and medicine. *J J. nanobiotechnology* 2, 1–6.

Sawant, S. (2017). "Development of biosensors from biopolymer composites," in *Biopolymer composites in electronics* (Elsevier), 353–383.

Senel, M., Dervisevic, M., and Kokkokoğlu, F. (2019). Electrochemical DNA biosensors for label-free breast cancer gene marker detection. *Anal. Bioanal. Chem.* 411, 2925–2935. doi:10.1007/s00216-019-01739-9

Shurbaji, S., Manaph, N. P. A., Ltaief, S. M., Al-Shammari, A. R., Elzatahry, A., and Yalcin, H. C. (2021). Characterization of MXene as a cancer photothermal agent under physiological conditions. *Front. Nanotechnol.* 63. doi:10.3389/fnano.2021.689718

Sobolčiak, P., Tanvir, A., Sadasivuni, K. K., and Krupa, I. (2019). Piezoresistive sensors based on electrospun mats modified by 2D Ti3C2Tx MXene. *Sensors (Basel).* 19, 4589. doi:10.3390/s19204589

Soundiraraju, B., and George, B. K. (2017). Two-dimensional titanium nitride (Ti2N) MXene: Synthesis, characterization, and potential application as surface-enhanced Raman scattering substrate. *ACS Nano* 11, 8892–8900. doi:10.1021/acsnano.7b03129

Sun, L., Fu, Q., and Pan, C. (2021). Hierarchical porous "skin/skeleton"-like MXene/biomass derived carbon fibers heterostructure for self-supporting, flexible all solid-state supercapacitors. *J. Hazard. Mat.* 410, 124565. doi:10.1016/j.jhazmat.2020.124565

Szuplewska, A., Kulpińska, D., Dybko, A., Jastrzębska, A. M., Wojciechowski, T., Rozmysłowska, A., et al. (2019a). 2D Ti2C (MXene) as a novel highly efficient and selective agent for photothermal therapy. *Mater. Sci. Eng. C* 98, 874–886. doi:10.1016/j.msec.2019.01.021

Szuplewska, A., Rozmysłowska-Wojciechowska, A., Poźniak, S., Wojciechowski, T., Birowska, M., Popielski, M., et al. (2019b). Multilayered stable 2D nano-sheets of Ti2NTx MXene: Synthesis, characterization, and anticancer activity. *J. Nanobiotechnology* 17, 114–14. doi:10.1186/s12951-019-0545-4

Tabadkani, M., Bani, N., Gharib, M., Ziaeemehr, A., Samadi, S., Rastgar-Moghadam, A., et al. (2021). Association between the Cx371019 C> T genetic variant and risk of breast cancer. *Meta Gene* 29, 100925. doi:10.1016/j.mgene.2021.100925

Tang, Q., Zhou, Z., and Chen, Z. J. N. (2013). *Graphene-related nanomaterials: tuning properties by functionalization*, 5, 4541–4583.

Tohme, S., Simmons, R. L., and Tsung, A. (2017). Surgery for cancer: A trigger for metastases. *Cancer Res.* 77, 1548–1552. doi:10.1158/0008-5472.can-16-1536

Urbankowski, P., Anasori, B., Makaryan, T., Er, D., Kota, S., Walsh, P. L., et al. (2016). Synthesis of two-dimensional titanium nitride Ti 4 N 3 (MXene). *Nanoscale* 8, 11385–11391. doi:10.1039/c6nr02253g

Vahidmohammadi, A., Hadjikhani, A., Shahbazmohamadi, S., and Beidaghi, M. (2017). Two-dimensional vanadium carbide (MXene) as a high-capacity cathode material for rechargeable aluminum batteries. *ACS Nano* 11, 11135–11144. doi:10.1021/acsnano.7b05350

Verger, L., Xu, C., Natu, V., Cheng, H.-M., Ren, W., and Barsoum, M. W. (2019). Overview of the synthesis of MXenes and other ultrathin 2D transition metal carbides and nitrides. *Curr. Opin. Solid State Mat. Sci.* 23, 149–163. doi:10.1016/j.cossms.2019.02.001

Waks, A. G., and Winer, E. P. (2019). Breast cancer treatment: A review. *J. Jama* 321, 288–300. doi:10.1001/jama.2018.19323

Wang, H., Sun, J., Lu, L., Yang, X., Xia, J., Zhang, F., et al. (2020). Competitive electrochemical aptasensor based on a cDNA-ferrocene/MXene probe for detection of breast cancer marker Mucin1. *Anal. Chim. Acta X.* 1094, 18–25. doi:10.1016/j.aca.2019.10.003

Wang, H., Wu, Y., Yuan, X., Zeng, G., Zhou, J., Wang, X., et al. (2018). Clay-inspired MXene-based electrochemical devices and photo-electrocatalyst: State-of-the-art progresses and challenges. *Adv. Mat.* 30, 1704561. doi:10.1002/adma.201704561

Wang, L., Zhang, H., Wang, B., Shen, C., Zhang, C., Hu, Q., et al. (2016). Synthesis and electrochemical performance of Ti3C2Tx with hydrothermal process. *Electron. Mat. Lett.* 12, 702–710. doi:10.1007/s13391-016-6088-z

Wang, X., and Cheng, L. J. N. (2019). Multifunctional two-dimensional nanocomposites for photothermal-based combined cancer therapy. *Nanoscale* 11, 15685–15708. doi:10.1039/c9nr04044g

Wang, X., Wang, X., Yue, Q., Xu, H., Zhong, X., Sun, L., et al. (2021a). Liquid exfoliation of TiN nanodots as novel sonosensitizers for photothermal-enhanced sonodynamic therapy against cancer. *Nano Today* 39, 101170. doi:10.1016/j.nantod.2021.101170

Wang, X., Zhong, X., and Cheng, L. J. C. C. R. (2021b). Titanium-based nanomaterials for cancer theranostics. *Coord. Chem. Rev.* 430, 213662. doi:10.1016/j.ccr.2020.213662

Wang, Y., Zeng, Z., Qiao, J., Dong, S., Liang, Q., and Shao, S. (2021c). Ultrasensitive determination of nitrite based on electrochemical platform of AuNPs deposited on PDDA-modified MXene nanosheets. *Talanta* 221, 121605. doi:10.1016/j.talanta.2020.121605

Wang, Z., Luan, J., Seth, A., Liu, L., You, M., Gupta, P., et al. (2021d). Microneedle patch for the ultrasensitive quantification of protein biomarkers in interstitial fluid. *Nat. Biomed. Eng.* 5, 64–76. doi:10.1038/s41551-020-00672-y

Williams, D. F. J. B. (2008). On the mechanisms of biocompatibility. *Biomaterials* 29, 2941–2953. doi:10.1016/j.biomaterials.2008.04.023

Woo, J. H., Kim, N. H., Kim, S. I., Park, O.-K., and Lee, J. H. (2020). Effects of the addition of boric acid on the physical properties of MXene/polyvinyl alcohol (PVA) nanocomposite. *Compos. Part B Eng.* 199, 108205. doi:10.1016/j.compositesb.2020.108205

Wu, Z., Shi, J., Song, P., Li, J., and Cao, S. (2021). Chitosan/hyaluronic acid based hollow microcapsules equipped with MXene/gold nanorods for synergistically enhanced near infrared responsive drug delivery. *Int. J. Biol. Macromol.* 183, 870–879. doi:10.1016/j.ijbiomac.2021.04.164

Xu, C., Wang, L., Liu, Z., Chen, L., Guo, J., Kang, N., et al. (2015). Large-area high-quality 2D ultrathin Mo2C superconducting crystals. *Nat. Mat.* 14, 1135–1141. doi:10.1038/nmat4374

Yang, X., Feng, M., Xia, J., Zhang, F., and Wang, Z. (2020). An electrochemical biosensor based on AuNPs/Ti3C2 MXene three-dimensional nanocomposite for microRNA-155 detection by exonuclease III-aided cascade target recycling. *J. Electroanal. Chem. (Lausanne).* 878, 114669. doi:10.1016/j.jelechem.2020.114669

Yin, H., Guan, X., Lin, H., Pu, Y., Fang, Y., Yue, W., et al. (2020). Nanomedicine-enabled photonic thermogaseous cancer therapy. *Adv. Sci. (Weinh).* 7, 1901954. doi:10.1002/advs.201901954

Yu, X., Cai, X., Cui, H., Lee, S.-W., Yu, X.-F., and Liu, B. (2017). Fluorine-free preparation of titanium carbide MXene quantum dots with high near-infrared photothermal performances for cancer therapy. *Nanoscale* 9, 17859–17864. doi:10.1039/c7nr05997c

Zada, S., Dai, W., Kai, Z., Lu, H., Meng, X., Zhang, Y., et al. (2020). Algae extraction controllable delamination of vanadium carbide nanosheets with enhanced near-infrared photothermal performance. *Angew. Chem. Int. Ed. Engl.* 59, 6663–6668. doi:10.1002/ange.201916748

Zeng, H., Deng, L., Yang, L., Wu, H., Zhang, H., Zhou, C., et al. (2021). Novel Prussian blue analogues@ MXene nanocomposite as heterogeneous activator of peroxymonosulfate for the degradation of coumarin: The nonnegligible role of Lewis-acid sites on MXene. *Chem. Eng. J.* 416, 128071. doi:10.1016/j.cej.2020.128071

Zhang, P., Yang, X.-J., Li, P., Zhao, Y., and Niu, Q. J. (2020). Fabrication of novel MXene (Ti 3 C 2)/polyacrylamide nanocomposite hydrogels with enhanced mechanical and drug release properties. *Soft Matter* 16, 162–169. doi:10.1039/c9sm01985e

Zhou, J., Zha, X., Chen, F. Y., Ye, Q., Eklund, P., Du, S., et al. (2016). A two-dimensional zirconium carbide by selective etching of Al3C3 from nanolaminated Zr3Al3C5. *Angew. Chem. Int. Ed. Engl.* 55, 5092–5097. doi:10.1002/ange.201510432

Zhu, B., Shi, J., Liu, C., Li, J., and Cao, S. (2021). *In-situ* self-assembly of sandwich-like Ti3C2 MXene/gold nanorods nanosheets for synergistically enhanced near-infrared responsive drug delivery. *Ceram. Int.* 47, 24252–24261. doi:10.1016/j.ceramint.2021.05.136